Application of an orbital radar sounder model to detecting Martian polar subsurface features

Yanbin Xu,[1] Steven A. Cummer,[1] and William M. Farrell[2]

Received 2 August 2005; revised 12 November 2005; accepted 6 January 2006; published 13 May 2006.

[1] A model to simulate the complete planetary orbital radar sounder problem is presented in this paper. The subsurface features and the ionosphere will not only bring ambiguity to the collected radar sounder data, but also critically affect instrument capabilities. These environmental uncertainties generate a compelling need for meaningful quantitative simulation of the orbital radar sounder problem. Our model combines finite difference time domain (FDTD) and analytical methods and splits the computational volume into two pieces owing to the large size of the simulation space. The near-surface and subsurface fields are computed with the FDTD method to improve the simulation flexibility of the surface and subsurface features. The two-way ionospheric propagation is treated with the simpler but accurate near-far field transformation method to maximize computational efficiency. With the capability of including all of the important radar sounder effects that can be difficult to compute analytically, the model enables accurate numerical experimentation with realistic instrumental and environmental parameters, and can handle an arbitrarily two-dimensionally inhomogeneous ground and an arbitrary ionospheric profile. Simulation results are given on the application of detecting Martian polar subsurface water, and we place bounds on the ionospheric losses and the subsurface conductivity through which water can be detected. We find that a basal lake located $\sim$2.5 km below the surface is near the limit of detectability. The ionospheric losses should be no larger than 10 dB and the average subsurface conductivity should be no larger than 4×10^{-6} S/m for the basal lake to be detectable.

Citation: Xu, Y., S. A. Cummer, and W. M. Farrell (2006), Application of an orbital radar sounder model to detecting Martian polar subsurface features, *J. Geophys. Res.*, *111*, E06S17, doi:10.1029/2005JE002547.

1. Introduction

[2] Exciting recent discoveries in planetary science have made subsurface exploration a very high priority on future missions. The discovery of water, in any phase, on non-terrestrial planetary bodies would have profound implications for many scientific disciplines. The apparent liquid run-off channels imaged by the Mars Orbiter Camera (MOC) on Mars Global Surveyor (MGS) [*Malin and Edgett*, 2000] are compelling but indirect evidence of geologically recent flowing liquid on the planet. Evidence for geological structure indicative of sedimentation from waves on large bodies of water [*Head et al.*, 1999] has also been found on Mars in laser altimeter data. Recent find of minerals jarosite and magnesium sulfate salts on Mars [*Vaniman et al.*, 2004; *Jakosky and Mellon*, 2004] agrees with early evidence of flowing liquid [*Baratoux et al.*, 2002] since the minerals require the presence of liquid water to form. However, the likely subsurface nature of any water on Mars makes it hard to find. Direct detection of water requires methods like drilling or penetration to make in situ measurements, which are extremely challenging from an engineering standpoint.

[3] Ground-penetrating radar (GPR) is a relatively mature technology for a variety of terrestrial subsurface remote sensing applications, and has also been applied to planetary remote sensing problems including search for subsurface water [*Beaty et al.*, 2000, 2001]. Orbiter and surface GPR instruments are already planned for current and future Mars missions, including MARSIS on Mars Express and SHARAD on the Mars Reconnaissance Orbiter. Orbital radar sounder has the advantage in planetary remote sensing since an instrument on an orbiter can probe a wide area of a planetary body. However, it will be operating in unknown environments, and these environments, such as ionosphere and subsurface features, critically affect instrument performance. As an example, a recent theoretical study has shown that the lower part of the Martian ionosphere, about which very little is known, may be a much better absorber of radar signals than previously thought [*Witasse et al.*, 2001]. These issues and others, such as the effect of a rough planetary surface, could severely affect the operation of the orbital radar sounder. A complete theoretical analysis of the orbital radar sounder problem is difficult, however, because of the wide variety of processes from subsurface electromagnetic

[1]Department of Electrical and Computer Engineering, Duke University, Durham, North Carolina, USA.
[2]NASA Goddard Space Flight Center, Greenbelt, Maryland, USA.

0148-0227/06/2005JE002547$09.00

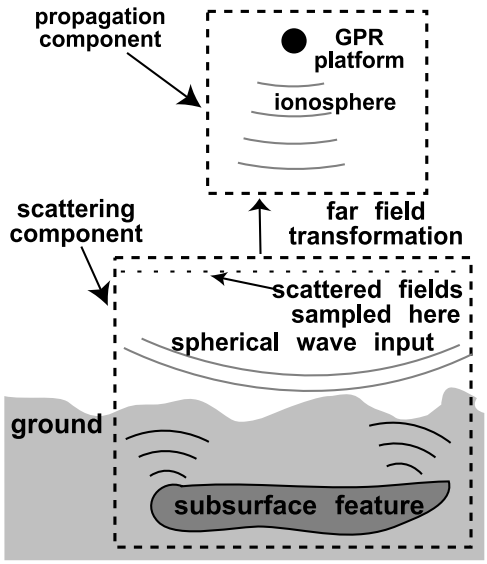

Figure 1. Schematic description of how the simulation is separated into the scattering component and the propagation component.

scattering to transionospheric pulse propagation that are important in the operation of the instrument.

[4] To help the data interpretation, GPR and radar sounder models have been developed. For example, *Heggy et al.* [2003] used the FDTD method to simulate the subsurface scattered fields from a lander-based GPR system. *Leuschen et al.* [2003] developed a simulator using a frequency domain algorithm to predict the performance of orbital radar sounder on Mars for various geological conditions that vary only in depth (one-dimensional (1-D)). *Farrell et al.* [2005] investigated the effect of ice reflective and conductive losses on the radar detection of subsurface water with a 1-D model and analytical methods. None of those radar sounder simulators includes the important ionospheric effects, which have impact on orbital radar sounder operation and data processing [*Safaeinili et al.*, 2003]. Although *Picardi et al.* [2004] considered the impact of ionosphere that was discussed by *Safaeinili et al.* [2003], their model can only solve problems with 1-D subsurface feature in depth. In this paper we present a model to simulate the complete orbital radar sounder problem, including ionospheric propagation, surface scattering, and subsurface scattering effects, in a full-wave model that can handle an arbitrarily two-dimensionally inhomogeneous ground and an arbitrary ionospheric profile. Such a model could quantify the detectability of key science targets, could quantify the effect of environmental uncertainties on radar sounder instruments, and would be valuable for the interpretation of planetary radar sounder data. Because Mars is of the primary interest here, the results presented focus on Mars-related issues. However, the model is sufficiently general to simulate the problem for any planetary environment.

2. Model Description

[5] Fundamentally, the orbital radar sounder transmits electromagnetic waves into the ground through the ionosphere. This energy will be reflected by any inhomogeneity in the subsurface electrical parameters including permittivity, permeability and conductivity. Some fraction of the subsurface reflected energy exits the ground, propagates through the ionosphere and finally is received by the radar sounder on the platform. The targeted subsurface inhomogeneities are not necessarily geometrically simple like a series of discrete layers. It is important to be able to calculate the scattered signals from objects like tilted layers or spatially limited objects to help interpret radar sounder data and help design the instrument. Numerical electromagnetic simulation techniques are necessary to develop an accurate tool for simulating realistic planetary orbital radar sounder problems.

[6] Our approach of using full-wave finite difference techniques ensures that the model is as general as possible, and that it realistically accounts for important effects like multiple scattering, layer tilt and surface roughness. However, owing to the long distance (typically many hundreds of wavelengths) between the radar sounder platform and the ground, the overall problem has a large size even for a two-dimensional subsurface. As a result, we use a modular approach to separate the simulation into two components that handle the surface and subsurface scattering portion (scattering component) and the ionospheric propagation portion (propagation component), as shown in Figure 1. In the scattering component, we use the finite difference time domain (FDTD) method [*Taflove and Hagness*, 2000; *Kunz and Luebbers*, 1993; *Yee*, 1966] to calculate the scattering surface and subsurface fields. In the propagation component, we use the simpler but accurate near-far field transformation method to treat the wave propagation through the ionosphere.

2.1. Scattering Component

[7] To simulate broadband fields in strongly inhomogeneous environments, numerical finite difference and related techniques are among the best choices. In the scattering component, we use the FDTD method to solve the surface and subsurface scattering fields. The FDTD method discretizes the computational domain into a grid of points, and the full fields are found at each grid point and discrete steps in time. The approach allows for maximum flexibility in the inhomogeneity of the surface and subsurface, and it can handle an arbitrarily time varying excitation with a single calculation. The inputs to the scattering component are the spherical incident waves above the ground surface and the subsurface electromagnetic parameters including permittivity, permeability, electric conductivity and magnetic loss. Because the source, in this case the orbital radar sounder, is far away from the surface, the incident waves above the ground surface are first analytically calculated and the total-field/scattered-field technique [*Taflove and Hagness*, 2000] is used to add the incident waves in the scattering component. The geoelectrical model is built by setting the subsurface electromagnetic parameters at each grid in the simulation space. The scattering component outputs the subsurface fields in a very small volume just above the ground. Those scattered fields are subsequently used as the input of the propagation component to simulate the return of the scattered fields to the receiver.

[8] The overall simulation is to compute fully 3-D fields from two-dimensionally inhomogeneous surface and subsurface. Owing to the large size of the problem, we use 2D FDTD to calculate the scattered fields, which satisfy the Maxwell's equations, assuming two dimensionally inhomogeneous ground and TM_z wave, as follows:

$$\mu\frac{\partial H_x}{\partial t}+\sigma^* H_x=-\frac{\partial E_z}{\partial y}, \tag{1}$$

$$\mu\frac{\partial H_y}{\partial t}+\sigma^* H_y=\frac{\partial E_z}{\partial x}, \tag{2}$$

$$\varepsilon\frac{\partial E_z}{\partial t}+\sigma E_z=\frac{\partial H_y}{\partial x}-\frac{\partial H_x}{\partial y}, \tag{3}$$

where E and H are the fields we solve, ε is the permittivity, μ is the permeability, σ is the electric conductivity and σ^* is the magnetic loss. We then transform the fields to 3-D in the propagation component. The scattering volume is truncated with a uniaxial perfectly matched layer (UPML) absorbing boundary condition [*Gedney*, 1996] to simulate the extension of the lattice to infinity and prevent unwanted reflections from the edges of the simulation space.

2.2. Propagation Component

[9] The subsurface fields at the edge of the volume in the scattering component are then used as the input to the propagation component to calculate the far fields that would be received by the radar sounder at higher altitudes. Because the orbiter is so distant from the ground, the propagation of the scattered energy back to the receiver can be complicated, particularly when the ionosphere is present between the orbiter and ground, which is the case for Mars and most planetary bodies. The free electrons in the ionosphere show their influence by imposing a cutoff frequency [*Budden*, 1985], below which electromagnetic waves are completely reflected by the plasma. This effect places a limit on the frequencies that can pass through the ionosphere either from above or from below. When a significant magnetic field is present, which is the case for localized regions of Mars [*Acuna et al.*, 1999], the propagation is further complicated by mode splitting with each mode having a different index of refraction and Faraday effect in which the linear polarization rotates with propagation distance [*Budden*, 1985]. Additionally, collisions between electrons and the neutral atmosphere dissipate electromagnetic wave energy and can substantially absorb waves passing through the ionosphere.

[10] One of the unique aspects of the model includes the simulation of important ionospheric effects like attenuation and dispersion. Whether or not the ionosphere is present, the spherical spreading of the energy exiting the ground and reaching the receiver also needs to be accounted for. This will be the case for any elevated platform, such as a balloon or satellite. We will use a near-far field transformation (equation (4)) to compute the fields at an arbitrary altitude from the fields just above the ground simulated by the scattering component and through an arbitrary ionospheric profile.

$$E_{far}=\frac{j}{\lambda}\iint E_{scat}(y,z)\frac{e^{-jkr}}{r}(\vec{a}_0\cdot\vec{r}_0)dydz, \tag{4}$$

where $k=\frac{\omega}{cn}$, with complex refractive index n as

$$n^2=1+\frac{\omega_p^2}{j\omega\upsilon-\omega(\omega\pm\omega_c)}, \tag{5}$$

where

$$\omega_p^2=N_e q^2/m_e\varepsilon \tag{6}$$

$$\omega_c=Bq/m_e. \tag{7}$$

Equation (4) is the formulation to calculate the far fields received by the receiver on the orbiter, and it implicitly assumes a slowly varying medium and neglects reflections. E_{scat} is the scattered fields just above the surface calculated by the scattering component and used as the input to the propagation component; λ is the wavelength and r is the distance between the receiver and the surface above the ground where the scattered fields E_{scat} are recorded; $\vec{r}_0$ is the unit vector pointing from surface to the receiver; and $\vec{a}_0$ is the unit normal of the planetary surface. The important ionospheric effects are included in the wave number k, where ω is the radio wave radian frequency and c is the speed of light. In equation (5), υ is the collision frequency, ω_p is the plasma radian frequency and ω_c is the cyclotron frequency of an electron moving in a magnetic field. Most of Mars (80%) has a magnetic field strength of less than 50 nT and even below 20 nT in the northern hemisphere which will allow unhindered operations for MARSIS [*Safaeinili et al.*, 2003]. In this situation, $\omega_c \ll \omega$ and can be neglected. In equation (6), N_e is the electron density in m^{-3}, q is the electron charge and equal to 1.6×10^{-19} C, m_e is the electron mass and equal to 9.1×10^{-31} kg and ε is the free space permittivity. B in equation (7) is the background magnetic field. By including the important ionospheric effects in the wave number k, the propagation component can simulate the scattered fields propagate through the ionosphere with an arbitrary profile.

[11] Theoretically, the integral in equation (4) should be done over the surface above all the illuminated area. For a single transmitted pulse, this area is very large and may be larger than hundreds of kilometers. For example, MARISIS has a 40-m dipole antenna and with a 3 MHz frequency, the one-way 3-dB beam width is estimated to be 2.5 rad. Supposing the altitude of MARSIS be 250 km, the illuminated area within the 3-dB beam width will have a ~200 km width in the along-track direction. To calculate the scattered fields over such a large surface like thousands of wavelengths for the MARSIS problem, the FDTD computation in the scattering component will be heavily burdened, and it requires a huge computer memory to complete the calculation. This is obviously inefficient and impractical for a simulator. However, we can take advantage of the fact that MARSIS will do pulse averaging over 100–150 pulses in

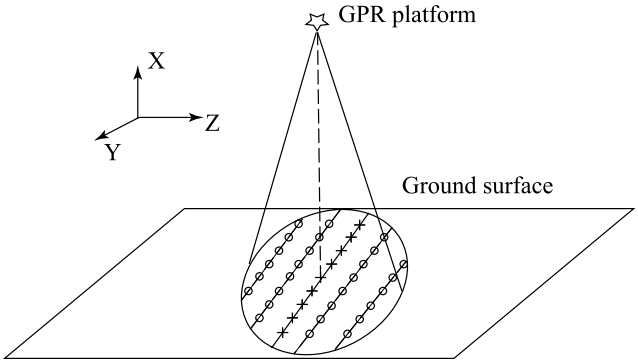

Figure 2. Near-far field transformation used to calculate the signal received by orbital radar sounder. Fields on the crossed line are calculated by the scattering component; fields on the circled line are estimated by adding a phase shift.

post signal processing. The synthesis of the signals produces the equivalent of an array antenna much longer than the real dipole antenna. Since MARSIS moves at 6 km/s and has a pulse repetition frequency (PRF) of 127 Hz [*Picardi et al.*, 2004], the length of the equivalent array antenna will be ~6 km. Also, the one-way 3-dB beam width of this equivalent array antenna is estimated by $\theta_{3dB} \cong \lambda/L$, where λ is the wavelength and L is the length of the equivalent array antenna [*Stimson*, 1998]. The 3-dB beam width is 0.016 rad and an altitude of 250 km gives a ~4 km width in the along-track direction. Since we assume that the subsurface is homogeneous in the cross-track direction, subsurface echoes from that direction should come from a small area at nadir. Therefore the signal components that contribute significantly to the averaged pulse should come from the ~4 km range in the along-track direction. Signal components coming beyond that area will be suppressed in the averaged pulse, and it is exactly the averaged pulse that scientists use to infer the Mars subsurface features. We therefore approximate equation (4) by only integrating over the surface within 10 km range to simulate the subsurface returns that contribute significantly to the averaged pulse. For orbital radar sounder at higher altitudes, larger areas may be needed to do the integral in equation (4), which can be estimated by the 3-dB beam width of the equivalent array antenna times the altitude of the orbital radar sounder.

[12] The overall simulation computes fully 3-D fields from two-dimensionally inhomogeneous surface and subsurface. Therefore, before we do the integral in equation (4), we need do 2-D to 3-D transformation for the scattered fields, as shown in Figure 2. Suppose the surface and subsurface are inhomogeneous in the y direction (along-track direction) but homogeneous in the z direction (cross-track direction). The 2D FDTD computation in the scattering component will be done in the xy plane and calculates the 2D scattered fields along the intersection line (crossed line) of the surface and the plane that is perpendicular to the surface and passes through the radar sounder platform. The scattered fields over the surface within 10 km range need to be estimated and the spherical spreading of the fields need to be included. We estimate the 3-D scattered fields on those lines (circled line) that are parallel to the intersection line by adding a spherical phase shift exp $(-jk\Delta d)$, where Δd id the difference of the distance to the orbital radar sounder between the location where we calculate the scattered fields and that we estimate the scattered fields. The resulting fields are

$$E(y,z) = E(y,z=0) * \frac{\exp\left(-jk\sqrt{h^2+y^2+z^2}\right)/\sqrt{h^2+y^2+z^2}}{\exp\left(-jk\sqrt{h^2+y^2}\right)/\sqrt{h^2+y^2}} \approx E(y,z=0) * \exp\left(-jk\left(\sqrt{h^2+y^2+z^2}-\sqrt{h^2+y^2}\right)\right). \quad (8)$$

Since we assume the subsurface is homogeneous along the z direction, the scattered fields on the circled lines are estimated by the calculated fields on the crossed line that have the same y coordinate. The change of the amplitude of the scattered fields has been neglected since the distance difference is too small compared to the distance between the orbital radar sounder and the surface, which is at least 250 km for MARSIS. Once we have the scattered fields over the surface within 10 km range, we can use equation (4) to find the far field at the orbital radar sounder.

[13] The surface echoes will contain both scattered fields from the nadir and incoherent scattering coming from the off-nadir illuminated area, known as clutter. Although we assume homogeneous subsurface in the cross-track direction, cross-track clutter from the surface is always there because no aperture synthesis is performed in that direction. In this paper we focus on the subsurface reflection components and neglect the surface clutter from the cross-track direction since we integrate the scattered fields over the surface within 10 km range. However, the clutter can be easily added to our simulation by surface response calculations [e.g., *Nouvel et al.*, 2004].

[14] To test the accuracy of the near- to far-field transformation in the propagation component of the code, we calculate the signal return reflected by an infinite perfect electrical conductor surface and compare the result to the analytical solution. We assume the transceiver is 250 km above the perfect electrical conductor and transmit a

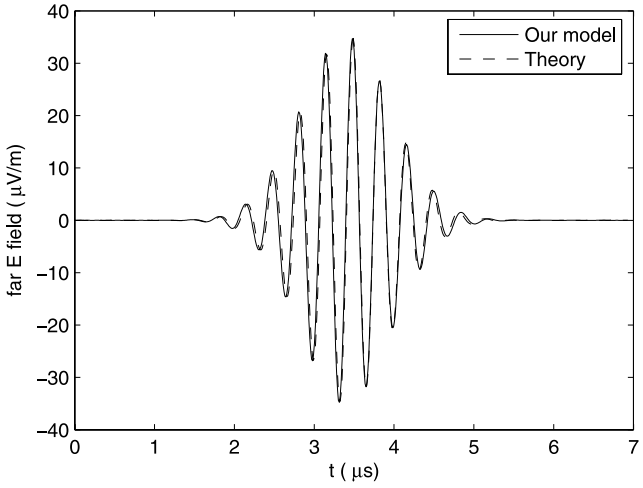

Figure 3. Backscattered fields by an infinite PEC calculated by our model compared to the theoretical result.

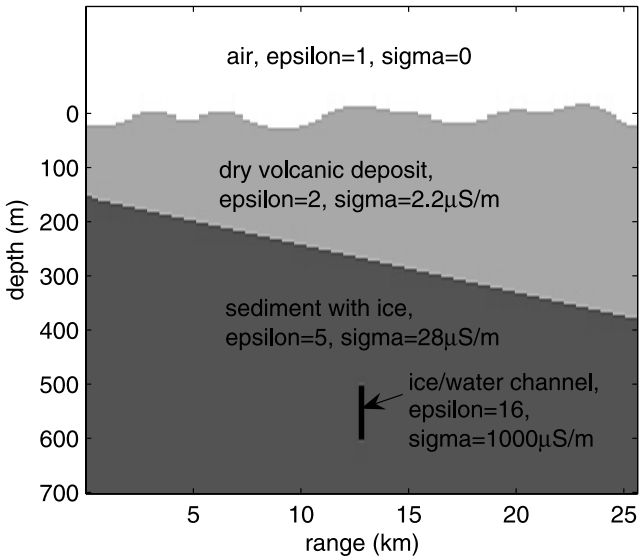

Figure 4. Geological model with surface roughness and clear 2D subsurface inhomogeneities.

MARSIS type pulse with 3-MHz central frequency, 1-MHz bandwidth and 10-W peak power. Figure 3 shows the received signal calculated by our model compared to the analytical solution.

3. Simulation Demonstration

[15] The primary scientific objective of MARSIS is to map the distribution and depth of the water/ice interface in the upper kilometers of the crust of Mars [*Picardi et al.*, 2004]. In subsurface sounding mode, the radar transmits a 1-MHz bandwidth pulse in four distinct bands: 1.3–2.3 MHz, 2.5–3.5 MHz, 3.5–4.5 MHz, and 4.5–5.5 MHz at the altitudes between 250 km and 800 km. The MARSIS instrument operates at 127.27-Hz pulse repetition frequency (PRF) to allow sufficient time for a single pulse roundtrip time for spacecraft altitudes as high as 800 km [*Safaeinili et al.*, 2003]. Since search for water on Mars is our current primary interest here, we will use a MARSIS type source in our simulation. However, our model is sufficiently general to simulate any orbital radar sounder transmitted signal for any planetary environment. In all of the following simulations we will assume the radar sounder platform altitude is 250 km. The transceiver operates at 3-MHz central frequency, the bandwidth is 1 MHz and the peak power is 10 W.

[16] As the first example, we will calculate the signal returns through free space and from a geological model with rough surface and clear 2D inhomogeneities including tilted layers and spatial limited objects. Figure 4 shows the modeled surface and subsurface. The rough surface of the top layer satisfies a Gaussian surface roughness spectrum [*Picardi et al.*, 2004]. The general procedure to generate this Gaussian rough surface is to randomly generate a surface spectrum that has Gaussian statistics and then inverse Fourier transform the spectrum to obtain a surface profile [*Thorsos*, 1988]. Data obtained by the Mars Orbiter Laser Altimeter (MOLA) suggest that the Mars surface is smooth in the vast northern hemisphere plains, where slopes are typically <0.5 degrees [*Aharonson et al.*, 2001]. We therefore set the RMS slope to be 0.5 degrees in the generated rough surface.

[17] The top layer of the geological model is made of dry volcanic deposit and the bottom layer is made of sediment with ice. The interface of the two layers has a ~0.5 degree slope, and electrical parameters of the layers are based on work by *Ciarletti et al.* [2003]. Suppose that there is a square ice/water channel (100 m by 100 m) in the sediment and the channel is the primary target of interest. Owing to the rough surface, the tilted layer and the spatially limited channel, 1-D algorithms like transmission line method will not work for this problem. However, our model can handle this problem easily because all those subsurface features can be included in the FDTD method by setting permittivity, permeability and conductivity at the corresponding position of the medium. Also, we set the FDTD cell size to be 2.5 m to satisfy at least 10 cells per wavelength. Figure 5 presents the simulated signal returns for a 2D radargram and all subsurface features like the tilted layer and the ice/water channel are reflected. We notice that ice/water channel reflection looks like a layer reflection. The reason is that the 250 km distance between the GPR platform and the ground is much larger than the scan path length that is about 10 km in the simulation. However, it is really the classic inverted-V signature of a discrete near-point subsurface scattering source with the inverted V stretched out. Also, this inverted-V signature is exactly what one would obtain because of the longer travel time for off-nadir target reflections.

4. Application to Polar Basal Lake Detection on Mars

[18] We will now apply our model to answering the question whether basal lakes at 2.5 km depth under the Mars north polar cap are detectable. Basal lakes are defined as water reservoirs formed at the underside of an ice mass and represent a key target for MARSIS during its northern

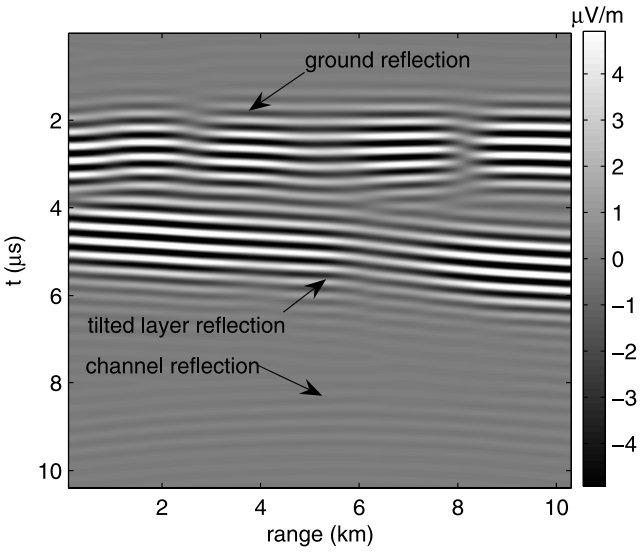

Figure 5. Simulated signal returns for a 2D radargram from the modeled subsurface.

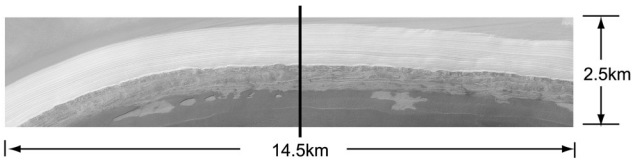

Figure 6. MGS/MOC image of Mars north polar layers (http://photojournal.jpl.nasa.gov/).

low-perigee polar overpasses. *Clifford* [1993] has described the possibility of such basal lake information under the Martian polar cap via melting from ice insulation effects, local geothermal hot spots, or heat-generating glacial sliding. Figure 6 is an MGS/MOC image of Mars north polar layered deposit (PLD) with ~14.5 km region of exposed terrain along Chasma Boreale (http://photojournal.jpl.nasa.gov/). The depth of the PLD layering is estimated to be ~2.5 km via scaling, assuming little/no foreshortening.

[19] The unique element of this image is that the sharp contrast of the layering. The brighter top region is suggestive of a set of ice/snow layers with a relatively low concentration of dust while the darker region has a large amount of sand. *Farrell et al.* [2005] assume that the image relative brightness indicates the concentration of dust in ice with larger brightness value meaning smaller sand concentration, and convert the brightness to permittivity and conductivity profiles. The permittivity values of the layers are obtained by directly mapping the brightness values of each pixel on the image, with upper ice layer brightness values (near data number 220 counts) being given a typical ice relative permittivity of 4 and lower sandy ice layer brightness values (near data number 130 counts) being given a typical sand relative permittivity of 5. The conductivity values of the layers are obtained in a similar way but with the consideration of temperature variation. The brightness values of the image are first linearly mapped to the sand concentration, and the sand concentration is then mapped to the conductivity on the basis of the model by *Chyba et al.* [1998]. Figure 7 shows the vertical profiles along a line in the middle of the image.

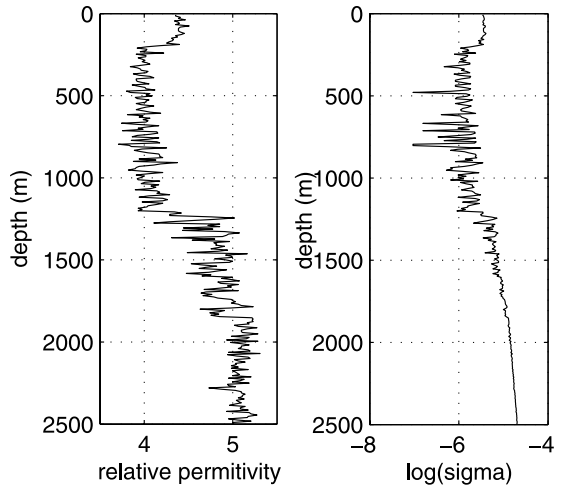

Figure 7. Vertical permittivity and conductivity profiles along a line in the middle of the image.

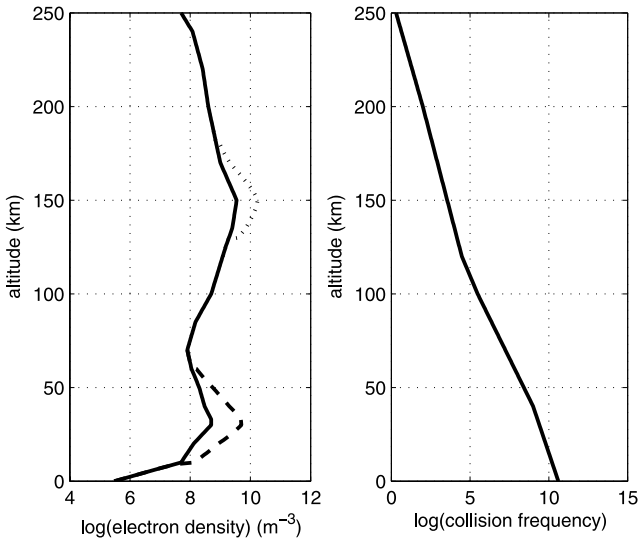

Figure 8. Mars nighttime ionosphere profiles. The dashed line shows an increase of 10 times of the peak electron density in the low Martian ionosphere (30 km), and the dotted line shows an increase of 5 times of the peak electron density in the high Martian ionosphere (150 km).

[20] The subsurface reflected signals can be weak because of the large distance of the orbiting platform. Ambient electromagnetic noise such as the cosmic background radiation may be comparable to the signal. MARSIS will use coherent pulse averaging to improve the SNR. Therefore we assume the noise level of the receiver is the cosmic background at 5 μV/m [*Novaco and Brown*, 1978]. The nighttime ionosphere profile [*Zhang et al.*, 1990] we use in the simulation is shown in Figure 8 (solid line). The character of this profile includes two electron density peaks, 3×10^9 m^{-3} at the altitude 150 km and 5×10^8 m^{-3} at 30 km. The attenuation essentially depends on the electron density profile over the bottom of the ionosphere due to large collision frequency at lower altitudes.

[21] Figure 9 is the simulation results of the 1-D radargram that compare the signal returns between propagation through free space and through the ionosphere based on the 1-D vertical permittivity and conductivity profiles along a line in the middle of the image (Figure 7). We focus on the ionospheric effects so that surface roughness is ignored in this example. The dielectric gradient has been included in our model for the subsurface layers above the basal lake since we extract the electrical parameters directly from the MOC image. The basal lake is modeled as a perfect electrical conductor to bound the upper limit of basal lake reflections. Sharp gradient and perfect electrical conductor give the most favorable condition for basal lake reflections. The basal lake dielectric gradient may be smooth and bake lakes may not be as reflecting as perfect electrical conductor. Either of these will reduce reflections. As shown in Figure 9, the peak of basal lake reflections is ~1 μV/m through free space and ~0.3 μV/m through the ionosphere. The two-way ionospheric effect on the signal is basically 10-dB attenuation and 5-μs time delay. No significant dispersion is introduced. That is because during nighttime the ionosphere has smaller electron density and hence night

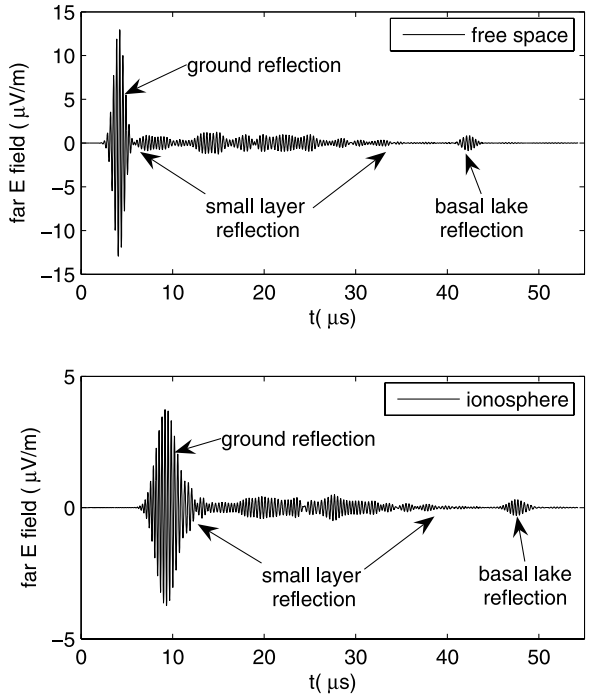

Figure 9. Simulation results for the 1-D radargram with the converted profiles.

is a good time for MARSIS subsurface sounding. Basal lakes at 2.5 km depth would be detectable since some SNR improving techniques such as pulse averaging can boost the SNR about 20 dB. In order to quantify the impact of low-altitude (30 km) ionospheric uncertainty, we assume that the peak electron density at 30 km altitude be 5×10^9 m^{-3} (dashed line in Figure 8), 10 times larger than the previously assumed value. Simulations show that the signal will attenuate another ~6 dB, which makes basal lakes hard to detect. As a comparison, increase of peak electron density at high altitude (150 km) by 5 times (dotted line in Figure 8) will also make the signal attenuate ~6 dB, with significant dispersion introduced. Therefore an ionosphere with the electron density peaks 3×10^9 m^{-3} at the altitude 150 km and 5×10^8 m^{-3} at 30 km puts basal lakes near the detectability limit. We also see some small layer reflections in the received signal as expected, which indicate that describing the subsurface feature with just two or three thick layers might not be accurate enough to calculate the signal returns and these small layer reflections may hinder the basal lake reflections.

[22] One of the goals to develop this simulation tool is to quantify the unknown environmental parameters for detectable science targets on the planetary body. We therefore examine the maximum of the average conductivity of the Mars north polar cap for basal lakes to be detectable. We run simulations as the average conductivity increases in a range from 10^{-7} S/m to 10^{-4} S/m and record the signal returns through free space for each value. The results are presented in Figure 10, which plots how the peak value of basal lake reflections changes with the subsurface average conductivity. The figure shows that the conductivity range between 10^{-5} S/m and 10^{-6} S/m is a critical range where the basal lake goes from undetectable to detectable for MARSIS, which agrees with the analysis by *Farrell et al.* [2004]. Although the peak goes below the cosmic background noise level when the conductivity increases to 1.8×10^{-6} S/m for one pulse, we still conclude that basal lakes are detectable if the average conductivity for the north polar cap is no larger than 4×10^{-6} S/m considering the possible 20-dB SNR improvement and 10 dB ionosphere attenuation.

[23] Finally, we simulate a 2D radargram over the north polar cap. The MOC image does not show any surface roughness but does show the roughness between subsurface layers. By using the 2D image as the input of the model and extracting the 2D subsurface electrical parameters from the image, the effects of the roughness between subsurface layers have been implicitly included in the simulation, which cannot be implemented in a 1-D simulator. The ground track length is 8 km as shown in the left panel in Figure 11. Also, the bright ice/snow layers tilt between the range 6 and 8 km. The right panel presents the signal returns received by the orbital radar sounder after propagating through the ionosphere. The simulation result shows a clear ground reflection and weak subsurface return. In order to clarify subsurface reflections, some colors have been made saturated in the figure. The basal lake reflections are ~0.3 μV/m, which is near the limit of detectability, when the subsurface in the nadir direction is pretty flat such as at the range of 3.5 km. The basal lake reflections are further reduced by a maximum of ~10 dB at the range of 8 km where the subsurface in the nadir direction has tilted layers. Therefore basal lake detectability is strongly dependent on the ionosphere and subsurface features. By including all these environments parameters in the simulation, our model can quantify the important environmental effects

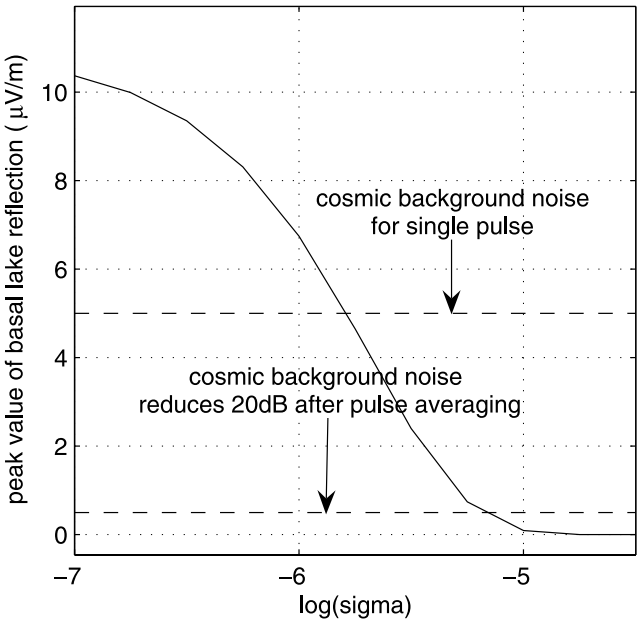

Figure 10. Estimation of the maximum of the average conductivity for detectable basal lakes.

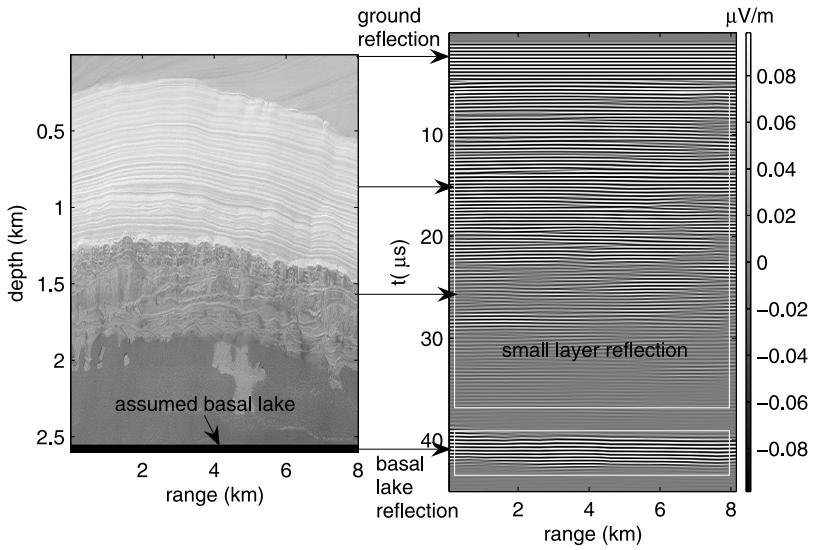

Figure 11. Simulation results for the 2D radargram over the Mars north polar cap. (Some of the colors are saturated to clarify basal lake reflections.)

on the signal returns and hence help data analysis and interpretation.

5. Conclusion

[24] In this paper we present a new simulation tool for planetary orbital radar sounder. Our model combines numerical and analytical methods and splits the computational volume into two pieces owing to the large size of the simulation space. The near-surface and subsurface fields are computed with the FDTD method to improve the simulation flexibility of the surface and subsurface features. The impact of ionosphere on signal returns is treated with simpler but accurate near-far field transformation method to maximize computational efficiency. Since search for water on Mars is one of the most important ongoing scientific missions, we apply our model to detecting basal lakes under the Mars north polar cap. We find that a basal lake located about 2.5 km below the surface is near the limit of detectability for the ionosphere with the peak electron density 3×10^9 m^{-3} at the altitude 150 km and 5×10^8 m^{-3} at 30 km. The ionospheric losses should be no larger than 10 dB and the average subsurface conductivity should be no larger than 4×10^{-6} S/m for the basal lake to be detectable. Ionosphere, small-layer reflection, tilted layer, rough surface and other environment unknowns may hinder the detection of water on Mars. With the capability of including all of these environmental effects that can be difficult to compute analytically, our model enables accurate numerical experimentation with realistic instrumental and environmental parameters.

[25] **Acknowledgment.** This research was supported by NASA Applied Information Systems Research Program grant NNG04GP83G.

References

Acuna, M. H., et al. (1999), Global distribution of crustal magnetization discovered by the Mars Global Surveyor MAG/ER experiment, *Science*, *284*, 790–793.

Aharonson, O., M. T. Zuber, and D. H. Rothman (2001), Statistics of Mars' topography from MOLA: Slopes, correlations, and physical models, *J. Geophys. Res.*, *106*, 723–737.

Baratoux, D., N. Mangold, C. Delacourt, and P. Allemand (2002), Evidence of liquid water in recent debris avalanche on Mars, *Geophys. Res. Lett.*, *29*(7), 1156, doi:10.1029/2001GL014155.

Beaty, D. W., et al. (2000), A strategic framework for the exploration of the Martian subsurface, technical report, Mars Program Off., Jet Propul. Lab., Pasadena, Calif.

Beaty, D. W., et al. (2001), Analysis of the potential of a Mars orbital ground-penetrating radar instrument in 2005, technical report, Mars Program Off., Jet Propul. Lab., Pasadena, Calif.

Budden, K. G. (1985), *The Propagation of Radio Waves*, Cambridge Univ. Press, New York.

Chyba, C. F., S. J. Ostro, and B. C. Edwards (1998), Radar detectability of a subsurface ocean on Europa, *Icarus*, *134*, 292–302.

Ciarletti, V., B. Martinat, A. Reineix, J. J. Berthelier, and R. Ney (2003), Numerical simulation of the operation of the GPR experiment on NETLANDER, *J. Geophys. Res.*, *108*(E4), 8028, doi:10.1029/2002JE001867.

Clifford, S. M. (1993), A model for the hydrological and climate behavior of water on Mars, *J. Geophys. Res.*, *98*, 10,973–11,016.

Farrell, W. M., J. J. Plaut, D. A. Gurnett, and G. Picardi (2004), Mars Express MARSIS radar: A prediction of the effect of overlaying ice on detecting polar basal lakes and inter-glacial aquifers, *NASA Tech. Memo.*, *NASA/TM-2004-212749*.

Farrell, W. M., J. J. Plaut, D. A. Gurnett, and G. Picardi (2005), Detecting sub-glacial aquifers in the North Polar layered deposits with Mars Express/MARSIS, *Geophys. Res. Lett.*, *32*, L11204, doi:10.1029/2005GL022488.

Gedney, S. D. (1996), An anisotropic perfectly matched layer absorbing media for the truncation of FDTD lattices, *IEEE Trans. Antennas Propag.*, *44*, 1630–1639.

Head, J. W., H. Hiesinger, M. A. Ivanov, M. A. Kreslavsky, S. Pratt, and B. J. Thomson (1999), Possible ancient oceans on Mars: Evidence from Mars Orbiter Laser Altimeter data, *Science*, *286*, 2134–2137.

Heggy, E., P. Paillou, F. Costard, N. Mangold, G. Ruffie, F. Demontoux, G. Grandjean, and J. M. Malezieux (2003), Local geoelectrical models of the Martian subsurface for shallow groundwater detection using sounding radars, *J. Geophys. Res.*, *108*(E4), 8030, doi:10.1029/2002JE001871.

Jakosky, B. M., and M. T. Mellon (2004), Water on Mars, *Phys. Today*, *57*, 71–76.

Kunz, K., and R. Luebbers (1993), *The Finite Difference Time Domain Method for Electromagnetics*, CRC Press, Boca Raton, Fla.

Leuschen, C., S. Clifford, and P. Gogineni (2003), Simulation of a surface-penetrating radar for Mars exploration, *J. Geophys. Res.*, *108*(E4), 8035, doi:10.1029/2002JE001875.

Malin, M. C., and K. S. Edgett (2000), Evidence for recent groundwater seepage and surface runoff on Mars, *Science*, *288*, 2330–2335.

Nouvel, J. F., A. Herique, W. Kofman, and A. Safaeinili (2004), Radar signal simulation: Surface modeling with the Facet Method, *Radio Sci.*, *39*, RS1013, doi:10.1029/2003RS002903.

Novaco, J. C., and L. W. Brown (1978), Nonthermal galactic emission below 10 megahertz, *Astrophys. J.*, *221*, 114–123.

Picardi, G., et al. (2004), Performance and surface scattering models for the Mars Advanced Radar for Subsurface and Ionosphere Sounding (MARSIS), *Planet. Space Sci.*, *52*, 149–156.

Safaeinili, A., W. Kofman, J. F. Nouvel, A. Herique, and R. L. Jordan (2003), Impact of Mars ionosphere on orbital radar sounder operation and data processing, *Planet. Space Sci.*, *51*, 505–515.

Stimson, G. (1998), *Introduction to Airborne Radar*, SciTech, Mendham, N. J.

Taflove, A., and S. C. Hagness (2000), *Computational Electrodynamics: The Finite-Difference Time-Domain Method*, Artech House, Norwood, Mass.

Thorsos, E. I. (1988), The validity of the Kirchhoff approximation for rough surface scattering using a Gaussian roughness spectrum, *J. Acoust. Soc. Am.*, *83*, 78–93.

Vaniman, D. T., D. L. Bish, S. J. Chipera, C. I. Fialips, J. W. Carey, and W. C. Feldman (2004), Magnesium sulphate salts and the history of water on Mars, *Nature*, *431*, 663–665.

Witasse, O., J. F. Nouvel, J. P. Lebreton, and W. Kofman (2001), HF radio wave attenuation due to a meteoric layer in the atmosphere of Mars, *Geophys. Res. Lett.*, *28*, 3039–3042.

Yee, K. S. (1966), Numerical solution of initial boundary value problems involving Maxwell's equations in isotropic media, *IEEE Trans. Antennas Propag.*, *14*, 302–307.

Zhang, M. H. G., J. G. Luhmann, and A. J. Kliore (1990), An observational study of the nightside ionospheres of Mars and Venus with radio occultation methods, *J. Geophys. Res.*, *95*(A10), 17,095–17,102.

S. A. Cummer and Y. Xu, Department of Electrical and Computer Engineering, Duke University, Durham, NC 27708, USA. (ybxu@ee.duke.edu)

W. M. Farrell, NASA Goddard Space Flight Center, Greenbelt, MD 20771, USA.